Available online at www.sciencedirect.com
ScienceDirect
Trans. Nonferrous Met. Soc. China 34(2024) 453−464
Transactions of Nonferrous Metals Society of China
www.tnmsc.cn

Interfacial heat transfer coefficient of aluminum alloy in contact solid solution treatment process

Xue-rong SU, Zhen-kun SONG, Zhi-qiang ZHANG

School of Materials Science and Engineering, Jilin University, Changchun 130022, China

Received 17 July 2022; accepted 31 December 2022

Abstract: The interfacial heat transfer coefficient (IHTC) values of 7075 aluminum alloy in contact solid solution treatment process at different pressures, surface roughnesses and temperatures were determined by using finite element (FE) simulation and inversion optimization (IO) method, and the effects of these factors on IHTC were analyzed. The results showed that the IHTC value first increased with the increase of pressure and then remained stable. The IHTC value decreased with the increase of surface roughness. The instantaneous IHTC value first increased and then decreased with increasing the plate temperature. Based on the integrating phenomenological laws of pressure, surface roughness and temperature, a multifactorial-influenced IHTC prediction model was established. It could be used to well predict the instantaneous IHTC value of the alloy under different conditions.

Key words: aluminium alloys; contact solid solution treatment; interfacial heat transfer coefficient; finite element analysis; inversion optimization

1 Introduction

With the rapid development of automobile industry, the problems of environment and energy are becoming more and more prominent [1]. One of the most important reasons for these problems is the emission of automobile exhaust [2,3]. Automobile material lightweight is a popular development direction of automobile lightweight to achieve the goal of energy conservation and emission reduction [4−6]. In particular, aluminum alloys are widely used as lightweight materials due to their low density, high strength and reusable characteristics [7,8]. The drawback is that aluminum alloys have poor ductility and formability at room temperature [9−11]. Fortunately, hot stamping−quenching process [12] solves this problem effectively. The solid solution treatment is the first step in the hot stamping process of aluminum alloy, thus it is very important to shorten the solutionizing time of aluminum alloy to improve the production efficiency of aluminum alloy parts [13]. Since the thermal conductivity of aluminum alloy is much higher than that of steel [14−16], the efficiency of contact solid solution treatment is much higher than that of traditional heating furnace solid solution treatment, which further improves the hot stamping process [17]. In the process of contact solid solution treatment, heat transfer will occur between the plate and tools. When the plate temperature, pressure, the roughness of the contact interface and other factors change, the temperature history of the plate will change greatly, thus affecting the microstructure and the properties of the plate. For the control of temperature field in heat transfer process, the most important thing is to determine the interfacial heat transfer coefficient (IHTC) in contact solid solution treatment.

IHTC is transient and affected by many factors [18]. Determining the IHTC is a complex problem involving geometry, machinery, thermal

Corresponding author: Zhi-qiang ZHANG, Tel: +86-13604424829, E-mail: zhangzq@jlu.edu.cn
DOI: 10.1016/S1003-6326(23)66410-6

analysis and other disciplines. At present, there are three main methods to obtain the instantaneous value of IHTC, namely heat balance method [19], Beck nonlinear estimation method [20] and finite element optimization method [21]. In order to determine the IHTC values in the hot stamping process, researchers at home and abroad have conducted many experimental studies using different technologies and materials. JAIN [22] used the self-made temperature measuring device to obtain the IHTC values between 2024-T4, 2024-O, 6061-O and 1100-O aluminum alloys and H-13 tool steel under different temperatures, pressures and lubrication conditions. The results show that the IHTC gradually increases with the increase of pressure and decreases with the decrease of yield strength of the plate. ZHAO et al [23] determined the IHTC values of 5083 aluminum alloy in air transfer stage and hot stamping stage under different test conditions by using heat balance method and Beck nonlinear estimation method. CHANG et al [24] took 22MnB5 boron steel as the research object. They obtained the value of IHTC by using Beck nonlinear estimation method and explored the influence of contact pressure and surface roughness on IHTC. MILKEREIT et al [25] explored the heat transfer process between USIBOR1500P boron steel and tools and analyzed the influence mechanism of temperature, pressure and gap on the IHTC value during hot stamping. WEN et al [26] developed a set of advanced temperature acquisition device in the hot stamping process of boron steel with Al−Si coating and proposed an inverse algorithm for determining IHTC value. LIU et al [27−32] obtained the IHTC value under different conditions by fitting the experimental data from the hot stamping experiment of aluminum alloy with the simulation data obtained by PAM STAMP software. An interactive model of pressure, plate thickness and lubricant was further developed to predict the evolution of IHTC. HU et al [33] analyzed the effects of temperature, pressure and oxide layer thickness on IHTC.

IHTC is an important thermophysical parameter to describe the heat transfer capacity between plate and tools [34]. At present, there are many studies on IHTC in forming process, but there is a lack of research on IHTC in heating process. Therefore, the contact solid solution treatment experiment of 7075-T6 aluminum alloy was carried out in this study and the IHTC values under different pressure, surface roughness and temperature conditions were determined by using the combination method of finite element simulation and inversion optimization. The influence mechanism of those factors on IHTC was also analyzed. The main innovation of this study is to try to obtain instantaneous IHTC under different conditions by integrating phenomenological laws of different influencing factors. The corresponding IHTC theoretical model was further developed and verified to be accurate.

2 Methods of determining IHTC value in contact solid solution treatment

2.1 Experimental procedures for contact solid solution treatment of aluminum alloys

The material used in this experiment was 7075-T6 aluminum alloy with a thickness of 2 mm, and the sample size was 60 mm × 60 mm. The chemical composition of the material is shown in Table 1. H13 tool steel was selected as the contact dies material. A hole with a diameter of 1.2 mm was machined on the bottom surface of the contact dies, and the tip of the hole was 2 mm away from the top surface of the die. A K-type thermocouple with a diameter of 1 mm was inserted into the hole to obtain the temperature of the die in the contact solid solution treatment. A spring was added beneath the thermocouple to make it contact closely with the die. The die temperature was controlled by the heat cartridges inserted into the die and the PID control system. The contact solid solution treatment device is shown in Fig. 1.

Figure 2 shows the data acquisition system of plate temperature. A blind hole with a diameter of 1.2 mm and a depth of 10 mm was drilled on the side of the plate. A K-typed thermocouple with a diameter of 1 mm was inserted and fixed in the hole with its head covered with appropriate amount of silicone grease. The other end of the thermocouple

Table 1 Chemical composition of 7075-T6 aluminum alloy (wt.%)

Si	Mn	Fe	Cr	Cu	Zn	Ti	Mg	Al
0.09	0.05	0.13	0.19	1.4	5.7	0.03	2.6	Bal.

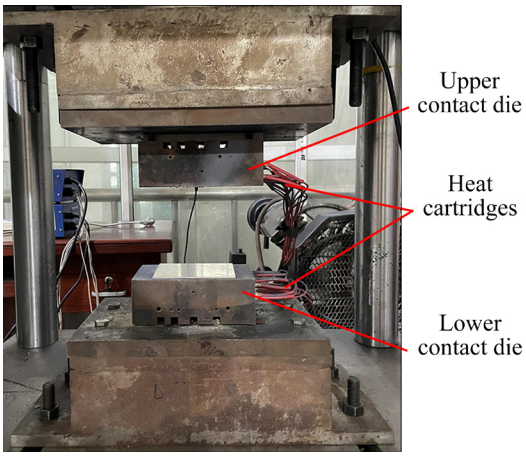

Fig. 1 Contact solid solution treatment device

was connected to the Yokogawa GM10 data acquisition instrument. The real-time temperature data was obtained through the communication between the computer and the GM10 acquisition. The temperature data were recorded 10 times/s.

The effects of pressure, surface roughness and plate temperature on the IHTC of 7075-T6 aluminum alloy in contact solid solution treatment were studied. In the experiment of exploring the influence of pressure, the contact dies temperature was set at 475 °C and the original plate without grinding was placed on the surface of the lower contact die. After the upper contact die was closed, load was exerted to make the pressure reach 10, 30, 50, 80, and 100 MPa. Each experiment was repeated three times for a total of 15 experiments. During the experiment on the influence of surface roughness, the contact dies temperature and the pressure were set at 475 °C and 50 MPa, respectively. The surfaces of 4 plates were ground with different types of sandpaper and then measured by a surface roughness measuring instrument. The types of sandpaper and the measured values of the corresponding surface roughness are shown in Table 2.

Figure 3 shows the temperature−time curves of plates in contact solid solution treatment process under different pressures and surface roughnesses. It can be seen that the slope of the curve is larger in the first 10 s, indicating that the heating rate of the plate increases rapidly in the early stage. After 10 s, the temperature curves gradually flatten out, and the heat balance between the plate and the contact dies is gradually achieved. The plate temperature changes greatly with the pressure less than 80 MPa, as shown in Fig. 3(a). Figure 3(b) shows the temperature data of the plate under different roughness conditions. Generally, the slope of the curve gradually decreases with increasing the surface roughness, indicating that the heating rate of plate gradually decreases, that is, the value of IHTC decreases with increasing the surface roughness.

2.2 Analysis model of heat transfer

According to the Fourier law and energy conservation law, the transient temperature field $T(x, y, z, t)$ (x, y and z are coordinates, and t is time) of the plate can be described as [35]

$$\frac{\partial}{\partial x}\left(\lambda\frac{\partial T}{\partial x}\right)+\frac{\partial}{\partial y}\left(\lambda\frac{\partial T}{\partial y}\right)+\frac{\partial}{\partial z}\left(\lambda\frac{\partial T}{\partial z}\right)+\rho Q=\rho c_p\frac{\partial T}{\partial t} \tag{1}$$

Fig. 2 Data acquisition system

Table 2 Types of sandpaper and roughnesses of sandpaper (R_a), original plate (R_s), and die surface (R_t) (μm)

Roughness of sandpaper, R_a				Roughness of original plate, R_s	Roughness of die surface, R_t
1200#	600#	180#	36#		
0.209	0.570	0.836	3.160	0.157	0.821

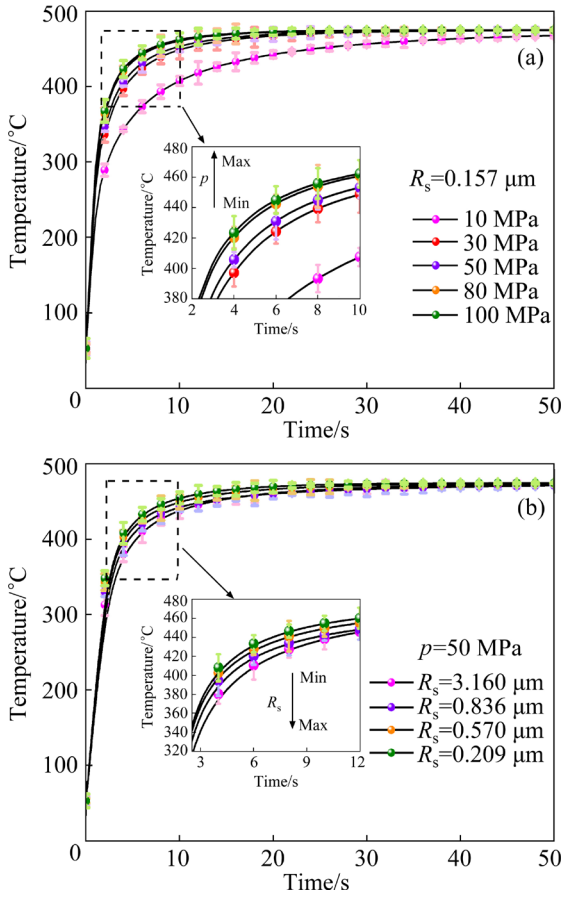

Fig. 3 Temperature−time curves of plates under different pressures (p) (a) and surface roughnesses (R_s) (b)

where λ is the thermal conductivity, W/(m·K); Q is the heat source intensity inside the plate, W/kg; ρ is the density of the plate, kg/m^3; c_p is specific heat capacity, J/(kg·K).

The initial condition is

$$T(x,y,z,t)\big|_{t=0}=T_0 \tag{2}$$

where T_0 is the initial temperature of the plate, °C.

Three types of boundary conditions (BC) can be described as follows:

The first type of BC is

$$T(x, y, z, t)=T_d \tag{3}$$

The second type of BC is

$$\lambda\left(\frac{\partial T}{\partial x}n_x+\frac{\partial T}{\partial y}n_y+\frac{\partial T}{\partial z}n_z\right)=q \tag{4}$$

The third type of BC is

$$\lambda\left(\frac{\partial T}{\partial x}n_x+\frac{\partial T}{\partial y}n_y+\frac{\partial T}{\partial z}n_z\right)=h\left(T_t-T_s\right) \tag{5}$$

where n_x, n_y and n_z are the direction cosine of the normal outside the boundary, T_d is the given temperature of the plate at the boundary, q is the heat flux density, h is the IHTC between the tool and the plate, and T_t and T_s are the surface temperatures of the tool and plate at the contact position, respectively.

In the present work, the thickness of the plate is only 2 mm, thus the heat transfer of the contact surfaces between the plate and the contact dies is much stronger than that between the non-contact surfaces of the plate and the air. Therefore, the contact solid solution process of the plate can be simplified as one-dimensional heat transfer along the z-axis. The contact dies are used as the external heat source of the plate (with constant temperature of T=475 °C). There is no internal heat source of the plate, thus Q can be set to be zero.

A heat transfer model was established with ABAQUS software to simulate the contact solid solution treatment of 7075-T6 aluminum alloy. The mesh model is shown in Fig. 4. There are 2980 elements of DC3D8 type in the whole model, including 2500 plate elements and 480 contact dies elements. It should be pointed out that when the plate is divided into 11250 elements, the simulation results are almost not different (as shown in Fig. 5). This indicates that the mesh has certain convergence when the number of elements is 2500. Therefore, in order to shorten the simulation time, 2500 elements are selected for the plate in the model. The thermophysical parameters of plate and dies are shown in Table 3. Since the contact dies temperature remains unchanged during the contact solid solution treatment process, all temperature values of the die are selected at 475 °C. In addition, temperature-related IHTC models were selected to investigate the influence of temperature on IHTC. The initial assumed values of IHTC at different temperatures are shown in Table 4. Since the final accurate values of IHTC are determined by

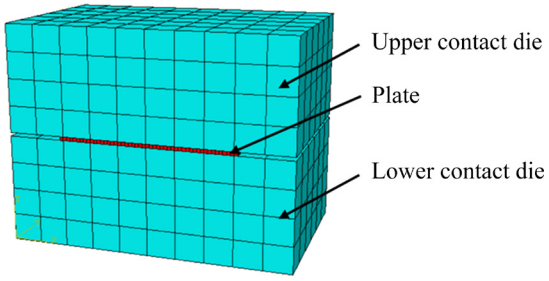

Fig. 4 Mesh diagram of heat transfer model

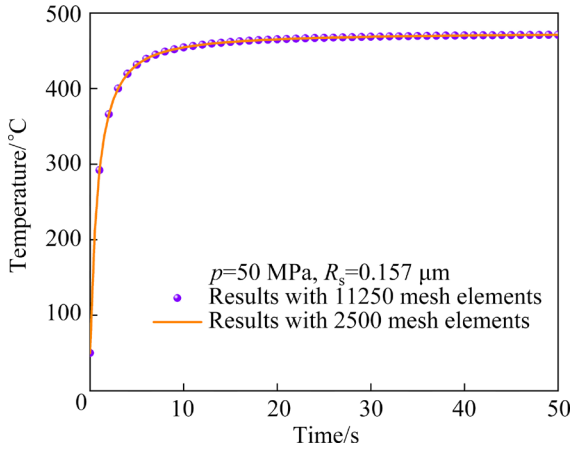

Fig. 5 Comparison of results at different numbers of mesh elements

Table 3 Thermophysical parameters of materials [26]

Parameter	Die	Plate
Material	H13	7075-T6
Specific heat capacity/ ($mJ·t^{-1}·°C^{-1}$)	$4.6×10^8$	$0.8721T^3−1462.5T^2+1.2×10^6T+6.083×10^8$
Density/($t·mm^{-3}$)	$7.8×10^{-9}$	$−6.7537×10^{-17}T^2−1.5×10^{-13}T+2.86×10^{-9}$
Conductivity/ ($mW·mm^{-1}·°C$)	28	$−5.145×10^{-5}T^2+0.1368T+85.224$
Initial temperature/°C	475	25

Table 4 IHTC values assumed during simulation

Plate temperature/°C	50	200	300	400	450	475
IHTC/($kW·m^{-2}·K^{-1}$)	0.6	3.5	4.0	3.5	2.5	0

optimization, the initial assumed values can be approximately given by referring to relevant articles.

Figure 6 shows the change history of plate temperature during simulation. Figure 6(a) shows the front view of the plate at different time, and Fig. 6(b) shows the top view of the plate when time is 34 s. As can be seen from Fig. 6(a), the plate temperature rises rapidly to higher than 400 °C during the time period of 0−7.5 s, and the heat transfer rate between the dies and the plate is large. The main reason is the large temperature difference between the dies of 475 °C and the plate of 25 °C. The heat flux passing through the plate per unit area is large in the process of heat transfer, thus the heating rate of the plate is fast. After 7.5 s, the plate temperature gradually rises with the extension of time and the dies temperature remains unchanged. Therefore, the temperature difference between the plate and the dies continues to decrease, resulting in the gradual decrease of the heating rate of the plate. After the solid solution treatment, the plate temperature is approximately 475 °C, which is in equilibrium with the die temperature, and thus the heat transfer process almost stops. It can be seen from Fig. 6(b) that the overall temperature of the plate is uniform after the solid solution treatment process.

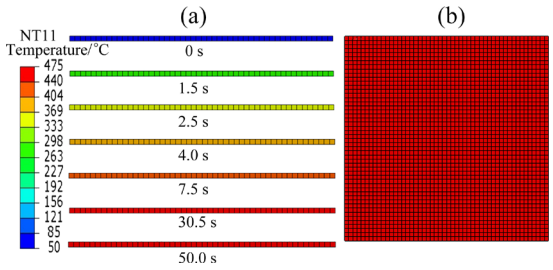

Fig. 6 Temperature change history of workpiece during simulation: (a) Front view of workpiece at different time; (b) Top view of workpiece at 34 s

After the simulation, the position on the plate consistent with the experimental measurement point was selected to output the temperature−time curve and compared with the experimental temperature−time curve, as shown in Fig. 7. Due to the inappropriate IHTC values, there is a large temperature difference between the simulated data and the experimental data. Therefore, further optimization of the IHTC values is needed to reduce the error.

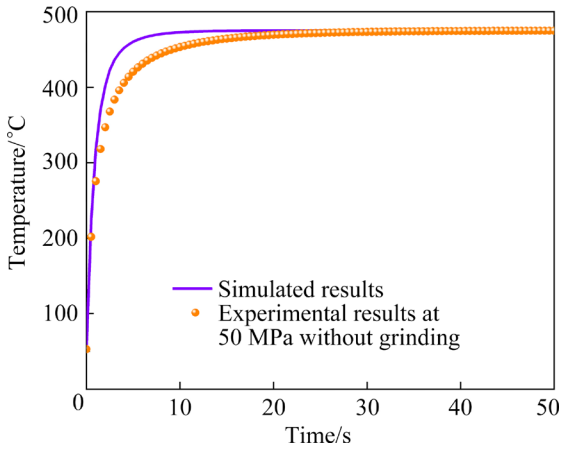

Fig. 7 Comparison of temperature data of plate between simulation and experiment

2.3 Inversion optimization of IHTC

The Mixed Integer Sequence Quadratic Programming (MISQP) algorithm in the Isight software was used to obtain the accurate values of IHTC in the contact solid solution treatment process of 7075-T6 aluminum alloy, taking the IHTC values as the design variable and the sum of the difference between the simulated data and the experimental data as the objective function for optimization calculation. The optimization equation can be described as

$$\begin{cases} \delta=\sum_{i=0}^{50}\left(T_i^{\mathrm{FEM}}-T_i^{\mathrm{EXP}}\right)^2=\delta_{\min} \\ \text{Constraint conditions:} \\ 0.1\leq h_1\leq 3.0,\ p=10\,\mathrm{MPa},R_{\mathrm{s}}=0.157\,\mu\mathrm{m} \\ 0.1\leq h_2\leq 4.5,\ p=50\,\mathrm{MPa},R_{\mathrm{s}}=0.157\,\mu\mathrm{m} \\ 0.1\leq h_3\leq 3.5,\ R_{\mathrm{s}}=0.209\,\mu\mathrm{m},\ p=50\,\mathrm{MPa} \\ 0.1\leq h_4\leq 2.5,\ R_{\mathrm{s}}=3.160\,\mu\mathrm{m},\ p=50\,\mathrm{MPa} \end{cases} \quad (6)$$

where T_i^{FEM} is the simulated temperature at different time; T_i^{EXP} is the experimental temperature at different time, and h_1, h_2, h_3 and h_4 are the IHTCs to be optimized under different experimental conditions, respectively.

The task flow diagram of the Isight interface consists of three modules (as shown in Fig. 8): ABAQUS, Data matching and Optimization. The Optimization component assigned values to IHTC according to the initial values, and then the ABAQUS component reoutputted the simulation data according to the assignment. The Data matching component read in the simulation data, calculating the deviation value from the experimental data and sending the results back to the Optimization module. The Optimization component reassigned a value in a given range to IHTC according to the feedback deviation value and then carried out the next round of optimization calculation until the error function reaches the minimum value. The flow chart of the optimization process is shown in Fig. 9. The essence of this optimization process is to explore the IHTC value which minimizes the objective function.

In order to verify the accuracy of the IHTC values determined by inversion optimization, the optimal IHTC values were substituted into the ABAQUS model again for numerical simulation to obtain the optimized temperature−time data of the plate. The comparison between the optimized temperature−time curve and the experimental temperature−time curve is shown in Fig. 10. It can be seen that the experimental and optimal curves fit well after the IHTC values were determined by inversion optimization (the deviation values were controlled within ±4.5 °C). Good experimental and optimized curves fitting results also show that the IHTC determination scheme based on temperature correlation adopted in this work is effective.

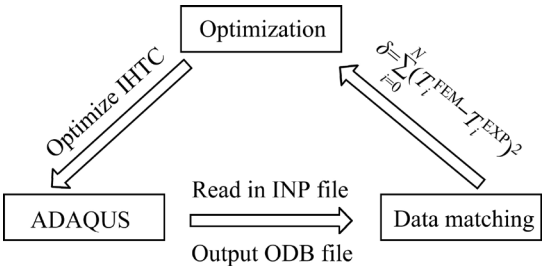

Fig. 8 Task flow chart in Isight interface

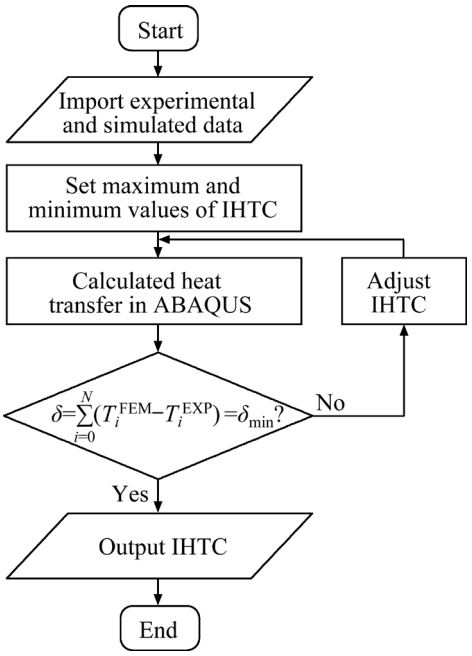

Fig. 9 Flow chart of optimizing IHTC

3 Results and discussion

3.1 Effect of pressure on IHTC

Figure 11 shows the average values of IHTC under different pressure conditions (R^2=0.95). The average IHTC has a nonlinear relationship with the pressure and approximately satisfies the following exponential function:

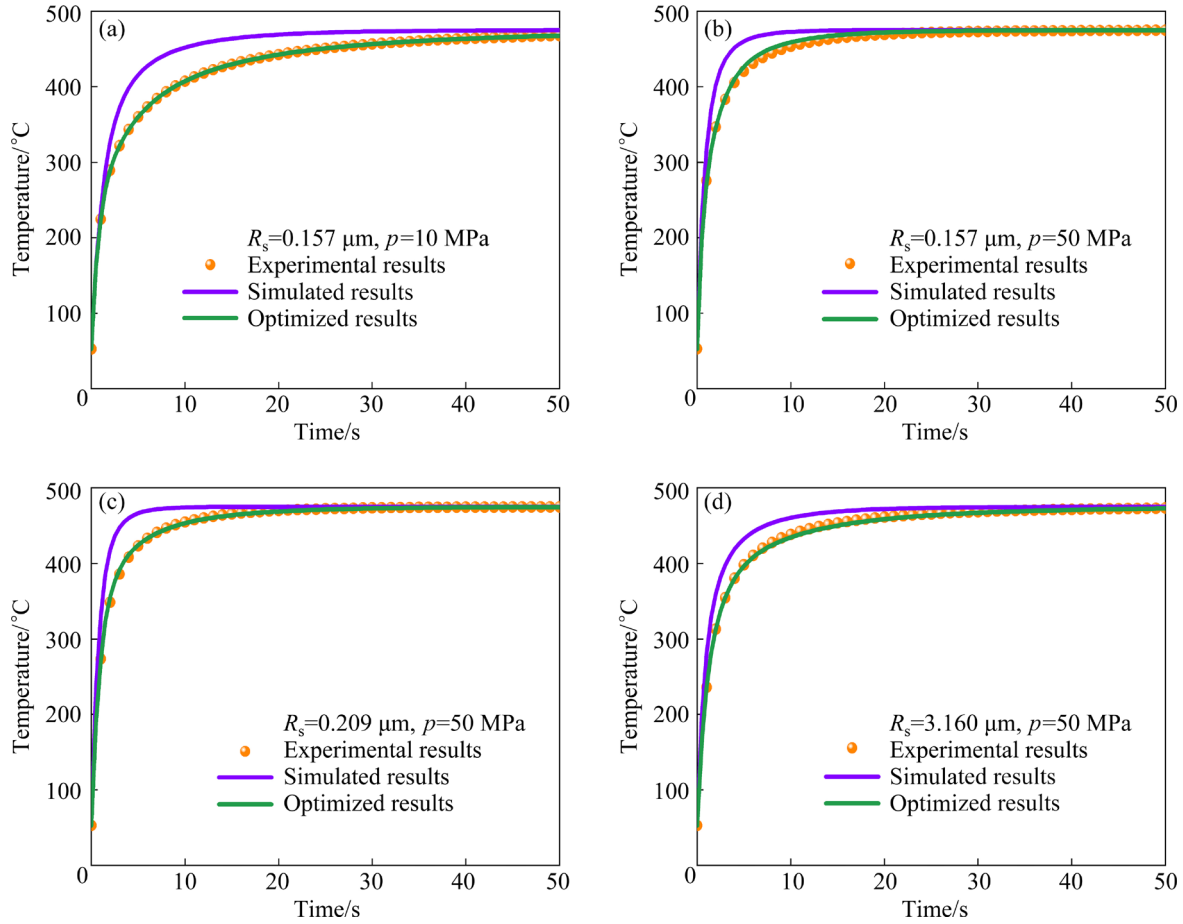

Fig. 10 Comparison of optimized data with experimental and simulated data under different conditions

$$h_p = -2.205\exp\left(-\frac{p}{39.619}\right)+3.387 \quad (7)$$

where h_p is the average IHTC.

The average IHTC between the plate and the contact dies increases from the initial 1.725 to 3.100 kW/(m^2·K) when the pressure increases from 10 to 80 MPa. When the pressure exceeds 80 MPa, the average IHTC increases a little and gradually tends to be stable. The reason is that with the increase of contact pressure, the asperities between the contact surface of the plate and the dies were crushed, which increased the effective contact area between the plate and the dies, and thus increased the IHTC values. However, after the contact pressure is greater than 80 MPa, the true contact area almost ceases to increase, so the IHTC remains basically unchanged.

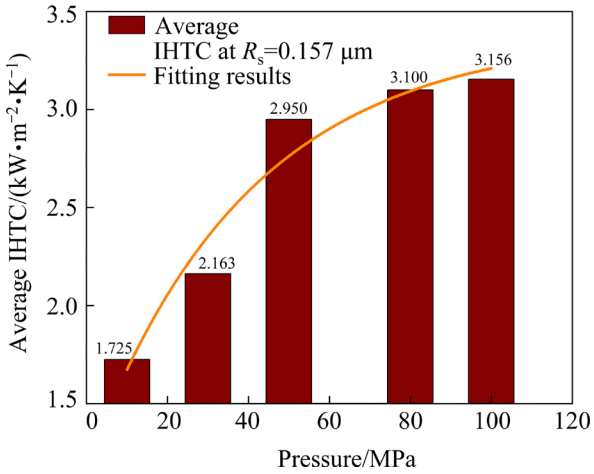

Fig. 11 Average IHTC under different pressure conditions

3.2 Effect of surface roughness on IHTC

Figure 12 shows the influence of surface roughness on average IHTC. By using the available functions to fit the data and compare the fitting results, it is concluded that the relationship between the average IHTC value (h_p) and the surface roughness of the plate approximately satisfies the following Allometric function:

$$h_p = 1.721\sqrt{\left(R_s^2 + R_t^2\right)^{-0.249}} \quad (8)$$

It should be pointed out that although a simple linear function can also get a good fitting effect, R^2=0.97, Allometric function has a better fitting effect, R^2=0.99. Since the fitting function will be used to develop the IHTC multifactorial model, the Allometric function is selected as the fitting result to avoid error accumulation.

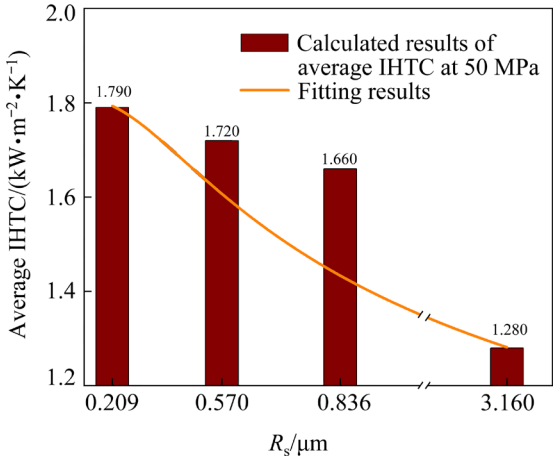

Fig. 12 Average IHTC under different surface roughness conditions

It can be seen that when the surface roughness of the plate increases from 0.209 to 3.160 μm, the average IHTC value decreases from 1.790 to 1.280 kW/(m^2·K). This is because sanding the surface of the plate with different types of sandpaper increases the number of micro bulges on the surface of the plate or increases the vertical height of the bulges, which reduces the effective contact area between the plate and the dies, leading to the reduction of IHTC values.

3.3 Effect of plate temperature on IHTC

Figure 13 shows the instantaneous IHTC change with plate temperature, and the influence of temperature on IHTC approximately satisfies the following Gauss function:

$$h_c = a - \frac{b}{c\sqrt{\pi/2}} \exp\left[-2\left(\frac{T-d}{c}\right)^2\right] \quad (9)$$

where h_c is instantaneous IHTC, and a, b, c and d are model parameters.

It can be seen that the variation trend of instantaneous IHTC with plate temperature is generally consistent under different pressure and roughness conditions. The instantaneous IHTC values first increase continuously to reach the peak

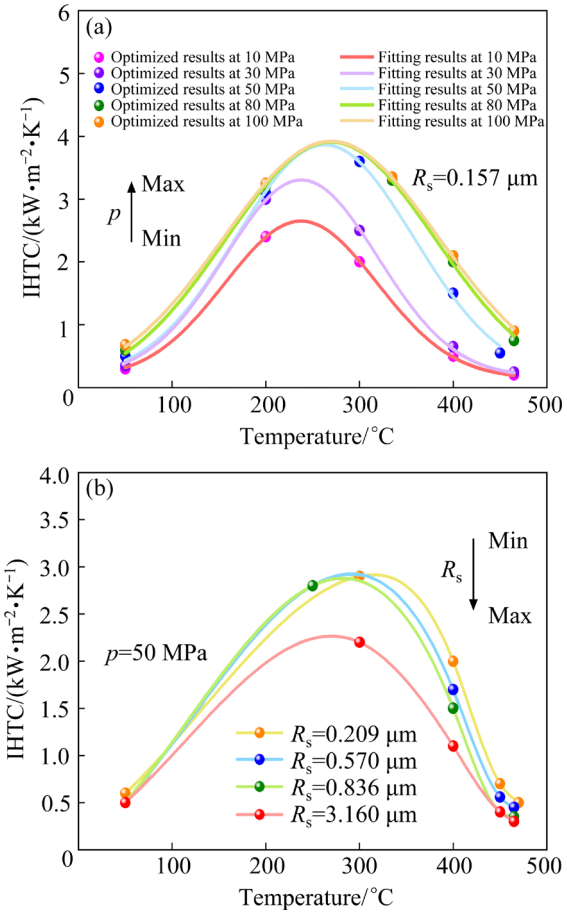

Fig. 13 Instantaneous IHTC with change of temperature at different pressures (a) and surface roughnesses (b)

value and then decrease gradually to almost 0 with the increase of plate temperature. The contact pressure can increase the effective contact area and has a positive effect on IHTC value, while the plate temperature has a negative impact on the IHTC value because the temperature difference between the plate and the dies decreases gradually with increasing the plate temperature. In the initial stage, the IHTC value increased continuously due to the increase of the effective contact area of the interface caused by gradual influence of the pressure. The IHTC reached the maximum value with the plate temperature rising to the range of 250−350 °C, as shown in Fig. 13(a). In this process, the positive influence of pressure on the instantaneous IHTC was greater than the negative impact of plate temperature. After the IHTC reached the peak value, the pressure had little effect on the instantaneous IHTC. At this time, the plate temperature continued to rise and the dies temperature was constant to be 475 °C, and thus the temperature difference between them gradually decreased. The negative

influence of the plate temperature on the instantaneous IHTC was in turn greater than the positive influence of the pressure, which caused the IHTC to gradually decrease until temperatures of the plate and contact dies were in thermal equilibrium and to be finally close to 0. The relationship between the instantaneous IHTC and the temperature of the plate under different surface roughnesses is basically the same as that for the change of pressure, shown in Fig. 13(b).

4 Development of multifactorial IHTC model

In order to better predict the instantaneous IHTC under different conditions, an IHTC multifactorial model based on the influence mechanism of multiple factors such as pressure, surface roughness and temperature was developed, as shown in Eq. (10):

$$h = Ak_{st}F(T)\frac{F(p)}{F(R_{st})} \tag{10}$$

where h is the IHTC, A is the model parameter, k_{st} is the harmonic average of the thermal conductivities of plate and contact dies, and $F(T)$, $F(p)$ and $F(R_{st})$ are the functions related to temperature, pressure and R_{st}, respectively,

$$k_{st}=\frac{2k_s k_t}{k_s+k_t} \tag{11}$$

$$R_{st}=\sqrt{R_s^2+R_t^2} \tag{12}$$

where k_s and k_t are the thermal conductivities of plate and dies, respectively.

$$F(T)=a-\frac{b}{c\sqrt{\pi/2}}\exp\left[-2\left(\frac{T-d}{c}\right)^2\right] \tag{13}$$

$$F(p)=a_0\exp\left(-\frac{p}{a_1}\right)+a_2 \tag{14}$$

where a_0, a_1 and a_2 are the model parameters.

$$F(R_{st})=R_{st}^{a_3} \tag{15}$$

where a_3 is the model parameter and R_{st} is the arithmetic square root of the sum of squares of the surface roughness of plate and dies.

The developed IHTC theoretical model involves a total of 9 parameters. Multiple groups of experimental data under different pressure, surface roughness and temperature conditions need to be used to optimize these parameters. 1stOpt software was used for calibrate the parameters. When the sum of the square of the error between the calculated and the optimized IHTC values reached the minimum, the calculation ended and a total of 19 iterative operations were carried out. The values of model parameters are shown in Table 5.

The comparison between the IHTC values calculated by the theoretical model and the IHTC values obtained by optimization is shown in Fig. 14. The sum of squares of the two errors is 2.5351 and the correlation coefficient R^2 is 0.9787, indicating that the developed model has high accuracy. In addition, IHTC is an important factor affecting the temperature history of plate, and a slight deviation will cause a significant change in the temperature−time curve. In order to further test the accuracy of the prediction about the instantaneous IHTC by the developed model in the contact solid solution treatment process of aluminum alloy, the IHTC values obtained by the model were substituted into ABAQUS software for simulation to obtain the corresponding temperature−time data which were used to compare with the experimental data. The results are shown in Fig. 15. It can be seen that the deviation between the calculated temperature and the experimental temperature is controlled within ±5 °C, and the fitting degree of the curve is high. Therefore, the developed multi-factor IHTC model can better predict the instantaneous IHTC values under different conditions.

Table 5 Values of model parameters

k_s/(kW·m^{-1}·K^{-1})	k_{st}/(kW·m^{-1}·K^{-1})	A	b	d	a_1	a_3
0.1395	0.047	3.4579	8308.87	524.33	57.6011	0.2862
k_t/(kW·m^{-1}·K^{-1})	R_t/μm	a	c	a_0	a_2	
0.028	0.821	−8.5607	−569.13	−0.0981	0.1594	

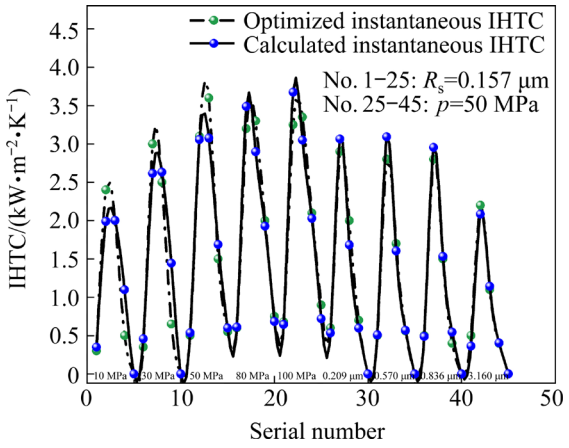

Fig. 14 Comparison of IHTC calculated by theoretical model and optimized

5 Conclusions

(1) In the process of contact solid solution treatment, the average IHTC between 7075-T6 aluminum alloy plate and dies first increased rapidly with the increase of pressure and then increased slowly after 50 MPa, and remained basically unchanged after 80 MPa. The average IHTC decreased with the increase of surface roughness. Under different pressures or roughnesses, the instantaneous IHTC began to increase with the rise of plate temperature, and then decreased with the rise of plate temperature.

(2) The inverse optimization of IHTC was carried out by using Isight software, and the optimized values of IHTC obtained under different experimental conditions were substituted into ABAQUS software for simulation again. Then, the corresponding temperature time data obtained were compared with the experimental data. The results showed that the deviation values were controlled within ±4.5 °C, and the overall fitting degree of the data curve was high, which verified that the IHTC values determined by inverse optimization were relatively accurate.

(3) Combining the influence mechanism of pressure, surface roughness and temperature on IHTC, a multi-factor IHTC model was developed, and the model parameters were optimized by 1stOpt software. The correlation coefficient R^2 in the result was 0.9787, with a high degree of fitting. In addition, the IHTC values calculated by the model

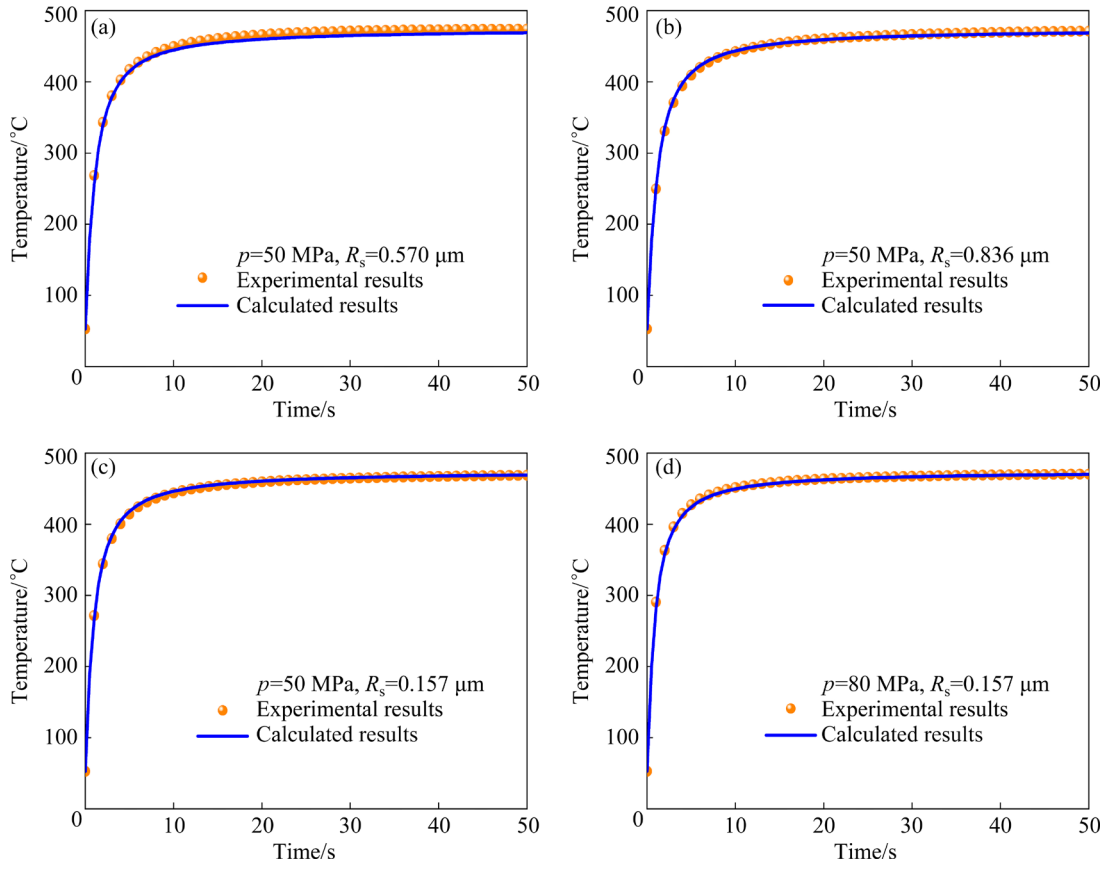

Fig. 15 Comparison between calculated results by theoretical model and experimental results under different conditions

were substituted into the ABAQUS software for simulation, and the corresponding temperature−time data were compared with the experimental data. The results showed that the deviation values were controlled within ±5 °C, which further verified the accuracy of the developed IHTC theoretical model.

CRediT authorship contribution statement

Xue-rong SU: Investigation, Formal analysis, Writing − Original draft; **Zhen-kun SONG:** Methodology, Resources, Software; **Zhi-qiang ZHANG:** Conceptualization, Supervision, Writing − Review & editing.

Declaration of competing interest

The authors declare that there are no known competing financial interests or personal relationships that could have appeared to influence the work reported in this paper.

References

[1] LOZHKIN V, LOZHKINA O, DOBROMIROV V. A study of air pollution by exhaust gases from cars in well courtyards of Saint Petersburg [J]. Transportation Research Procedia, 2018, 36: 453−458.

[2] DEGRAEUWE B, THUNIS P, CLAPPIER A, WEISS M, LEFEBVRE W, JANSSEN S, VRANCKX S. Impact of passenger car NO_x emissions and NO_2 fractions on urban NO_2 pollution—Scenario analysis for the city of Antwerp, Belgium [J]. Atmospheric Environment, 2016, 126: 218−224.

[3] DEGRAEUWE B, THUNIS P, CLAPPIER A, WEISS M, LEFEBVRE W, JANSSEN S, VRANCKX S. Impact of passenger car NO_x emissions on urban NO_2 pollution—Scenario analysis for 8 European cities [J]. Atmospheric Environment, 2017, 171: 330−337.

[4] XU Xiang, CHEN Xin-bo, LIU Zhe, XU Ya-nan, ZHANG Yong. Reliability-based design for lightweight vehicle structures with uncertain manufacturing accuracy [J]. Applied Mathematical Modelling, 2021, 95: 22−37.

[5] BEYENE A T, KORICHO E G, BELINGARDI G, MARTORANA B. Design and manufacturing issues in the development of lightweight solution for a vehicle frontal bumper [J]. Procedia Engineering, 2014, 88: 77−84.

[6] GOLOVASHCHENKO S F, WANG N, LE Q. Trimming and sheared edge stretchability of automotive 6xxx aluminum alloys [J]. Journal of Materials Processing Technology, 2018, 264: 64−75.

[7] ZHOU Bing, LU Shuai, XU Kai-le, XU Chun, WANG Zhan-yong, WANG Bin-jun. Hot cracking tendency test and simulation of 7075 semi-solid aluminium alloy [J]. Transactions of Nonferrous Metals Society of China, 2020, 30(2): 318−332.

[8] LIU J, CHENG Y S, CHAN S W N, SUNG D. Microstructure and mechanical properties of 7075 aluminum alloy during complex thixoextrusion [J]. Transactions of Nonferrous Metals Society of China, 2020, 30(12): 3173−3182.

[9] XU Xiao-feng, ZHAO Yu-guang, WANG Xu-dong, ZHANG Yang-yang, NING Yu-heng. Effect of rapid solid−solution induced by electropulsing on the microstructure and mechanical properties in 7075 Al alloy [J]. Materials Science and Engineering: A, 2016, 654: 278−281.

[10] GREZE R, MANACH P Y, LAURENT H, THUILLIER S, MENEZES L F. Influence of the temperature on residual stresses and springback effect in an aluminium alloy [J]. International Journal of Mechanical Sciences, 2010, 52(9): 1094−1100.

[11] DONG Guo-jiang, CHEN Zhi-wei, YANG Zhuo-yun, FAN Bo-cheng. Comparative study on forming limit prediction of AA7075-T6 sheet with M−K model and Lou−Huh criterion [J]. Transactions of Nonferrous Metals Society of China, 2020, 30(6): 1463−1477.

[12] FAN Xiao-bo, HE Zhu-bin, YUAN Shi-jian, ZHENG Kai-lun. Experimental investigation on hot forming−quenching integrated process of 6A02 aluminum alloy sheet [J]. Materials Science and Engineering: A, 2013, 573: 154−160.

[13] HUO Wang-tu, HOU Long-gang, ZHANG Yu-sheng, ZHANG Ji-shan. Warm formability and post-forming microstructure/property of high-strength AA 7075-T6 Al alloy [J]. Materials Science and Engineering: A, 2016, 675: 44−54.

[14] ZHANG Zhi-qiang, YU Jian-hao, HE Dong-ye. Influence of contact solid−solution treatment on microstructures and mechanical properties of 7075 aluminum alloy [J]. Materials Science and Engineering: A, 2019, 743: 500−503.

[15] ZHANG Zhi-qiang, YU Jian-hao, HE Dong-ye. Effect of contact solid solution treatment on peak aging of Al−Zn−Mg−Cu alloys [J]. Journal of Materials Research and Technology, 2020, 9(3): 6940−6943.

[16] ZHANG Zhi-qiang, YU Jian-hao, HE Dong-ye. Effects of contact body temperature and holding time on the microstructure and mechanical properties of 7075 aluminum alloy in contact solid solution treatment [J]. Journal of Alloys and Compounds, 2020, 823: 153919.

[17] RASERA J N, DAUN K J, SHI C J, D'SOUZA M. Direct contact heating for hot forming die quenching [J]. Applied Thermal Engineering, 2016, 98: 1165−1173.

[18] CHANG Ying, LI Xiao-dong, WANG Cun-yu, ZHENG Guo-jun, REN Da-xin, HU Ping, DONG Han. Determination of interfacial heat transfer coefficient and analysis of influencing factors in warm forming the third-generation automotive medium-Mn steel [J]. International Communications in Heat and Mass Transfer, 2017, 86: 108−116.

[19] ZHAO Kun-min, WANG Bin, CHANG Ying, TANG Xing-hui, YAN Jian-wen. Comparison of the methods for calculating the interfacial heat transfer coefficient in hot stamping [J]. Applied Thermal Engineering, 2015, 79: 17−26.

[20] BILAL M U, HORT N. Predicting the interfacial heat transfer coefficient of cast Mg−Al alloys using Beck's inverse analysis [J]. IOP Conference Series: Materials Science and Engineering, 2020, 861: 012027.
[21] HUNG T H, TSAI P W, CHEN F K, HUANG T B, LIU W L. Measurement of heat transfer coefficient of boron steel in hot stamping [J]. Procedia Engineering, 2014, 81: 1750−1755.
[22] JAIN V K. Determination of heat transfer coefficient for forging applications [J]. Journal of Materials Shaping Technology, 1990, 8(3): 193−202.
[23] ZHAO Kun-min, REN Da-xin, WANG Bin, CHANG Ying. Investigation of the interfacial heat transfer coefficient of sheet aluminum alloy 5083 in warm stamping process [J]. International Journal of Heat and Mass Transfer, 2019, 132: 293−300.
[24] CHANG Ying, TANG Xing-hui, ZHAO Kun-min, HU Ping, WU Yu-cheng. Investigation of the factors influencing the interfacial heat transfer coefficient in hot stamping [J]. Journal of Materials Processing Technology, 2016, 228: 25−33.
[25] MILKEREIT B, KESSLER O, SCHICK C. Recording of continuous cooling precipitation diagrams of aluminium alloys [J]. Thermochimica Acta, 2009, 492(1): 73−78.
[26] WEN Shuang, CHEN Zhen, QU Shao-fei, TANG J J, HAN Xian-hong. Investigations on the interfacial heat transfer coefficient during hot stamping of ultra-high strength steel with Al−Si coating [J]. International Journal of Heat and Mass Transfer, 2022, 189: 122739.
[27] LIU Xiao-chun, FAKIR O E, MENG Li-chun, SUN Xiao-guang, LI Xiao-dong, WANG Li-liang. Effects of lubricant on the IHTC during the hot stamping of AA6082 aluminium alloy: Experimental and modelling studies [J]. Journal of Materials Processing Technology, 2017, 255: 175−183.
[28] LIU Xiao-chun, JI Kang, FAKIR O E, FANG Hao-miao, GHARBI M M, WANG Li-liang. Determination of the interfacial heat transfer coefficient for a hot aluminium stamping process [J]. Journal of Materials Processing Technology, 2017, 247: 158−170.
[29] LIU Xiao-chun, FAKIR O E, ZHENG Yang, GHARBI M M, WANG Li-liang. Effect of tool coatings on the interfacial heat transfer coefficient in hot stamping of aluminium alloys under variable contact pressure conditions [J]. International Journal of Heat and Mass Transfer, 2019, 137: 74−83.
[30] JI Kang, LIU Xiao-chun, FAKIR O E, LIU Jun, ZHANG Qun-li, WANG Li-liang. Determination of the interfacial heat transfer coefficient in the hot stamping of AA7075 [J]. Manufacturing Review, 2016, 3: 5.
[31] LIU Xiao-chun, FAKIR O E, CAI Zhao-heng, DALKAYA B, WANG Ke-huan, GHARBI M M, WANG Li-liang. Development of an interfacial heat transfer coefficient model for the hot and warm aluminium stamping processes under different initial blank temperature conditions [J]. Journal of Materials Processing Technology, 2019, 273: 116245.
[32] LIU Xiao-chun, GHARBI M M, MANASSIB O, FAKIR O E, WANG Li-liang. Determination of the interfacial heat transfer coefficient between AA7075 and different forming tools in hot stamping processes [J]. Procedia Engineering, 2017, 207: 717−722.
[33] HU Ping, YING Liang, LI Ye, LIAO Zheng-wei. Effect of oxide scale on temperature-dependent interfacial heat transfer in hot stamping process [J]. Journal of Materials Processing Technology, 2013, 213(9): 1475−1483.
[34] JIANG Y F, DING H. Investigations of interfacial heat transfer efficiency in HFQ process of high strength aluminum alloy [J]. Materials Research Express, 2021, 8(1): 016507.
[35] KANG Lei, ZHAO Gang, TIAN Ni, ZHANG Hai-tao. Computation of synthetic surface heat transfer coefficient of 7B50 ultra-high-strength aluminum alloy during spray quenching [J]. Transactions of Nonferrous Metals Society of China, 2018, 28(5): 989−997.

铝合金在接触固溶处理工艺中的界面传热系数

苏雪荣，宋振坤，张志强

吉林大学 材料科学与工程学院，长春 130022

摘　要：采用有限元模拟和反演优化(IO)方法测定 7075 铝合金在不同压力、表面粗糙度和温度下接触固溶处理过程中的界面传热系数(IHTC)值，并分析这些因素对 IHTC 的影响。结果表明：随着压力的增加，IHTC 值先增加，然后保持稳定；IHTC 值随表面粗糙度的增大而减小；随着板温的升高，瞬时 IHTC 值先增大后减小。基于压力、表面粗糙度和温度的综合影响规律，建立多因素影响的 IHTC 理论模型。使用此模型能较好地预测不同条件下合金的瞬时 IHTC 值。

关键词：铝合金；接触固溶处理；界面传热系数；有限元分析；反演优化

(Edited by Wei-ping CHEN)